Inorganic Chemistry

Article

pubs.acs.org/IC

Synthesis and Structures of 9-Oxabispidine Analogues of Cisplatin, Carboplatin, and Oxaliplatin

David Pollak, Richard Goddard, and Klaus-Richard Pörschke*

Max-Planck-Institut für Kohlenforschung, Kaiser-Wilhelm-Platz 1, 45470 Mülheim an der Ruhr, Germany

Supporting Information

ABSTRACT: The literature synthesis of 9-oxabispidine [$OC_6H_{10}(NH)_2$, **C**] has been revisited and optimized, which includes determination of the crystal structures of **C**, the secondary component *trans*-$(PhSO_2)NC_4H_6O(CH_2I)_2$ (**trans-III**), and the unexpected solute intermediate $OC_6H_{10}(NSO_2Ph)_2 \cdot {}^1/_2py$ (**V·$^1/_2$py**). The reaction of (1,5-hexadiene)platinum dichloride with **C** yields $\{OC_6H_{10}(NH)_2\}PtCl_2$ (**C1**), which is converted to $\{OC_6H_{10}(NH)_2\}$-Pt(cbdca)·$5H_2O$ (**C2**) and $\{OC_6H_{10}(NH)_2\}Pt(C_2O_4)$ (**C3**). In the crystal, **C1** forms a planar 2D network by N−H··Cl and N−H··O hydrogen bonding. In the crystal structure of **C2**, which is isomorphous to the parent bispidine compound (**A2**), all complex molecules are encapsulated by a water shell. While complexes **C1** and **C3** are virtually insoluble in water, **C2** dissolves quite well. The low cytotoxicity of compounds **C1**−**C3** is explained by an increased polarity of the bonds in the **C** skeleton as a consequence of the electronegative O atom.

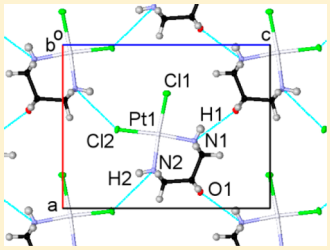

1. INTRODUCTION

The serendipitous discovery of the cytostatic properties of cisplatin, *cis*-$(NH_3)_2PtCl_2$, by Rosenberg and co-workers[1] in the mid-1960s has unleashed an enduring interest in the advancement of Pt-based anticancer drugs. The most notable developments were carboplatin, in which the labile chloride anions of cisplatin are replaced by 1,1-cyclobutanedicarboxylate (cbdca),[2] and oxaliplatin, *trans*-(*R*,*R*)-1,2-diaminocyclohexaneplatinum(II) oxalate.[3] Until today, these three compounds represent the only worldwide-approved platinum drugs for cancer therapy (Chart 1).

Chart 1. Worldwide-Approved Platinum Drugs for Cancer Therapy

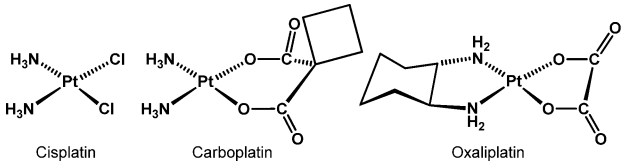

There are numerous serious side effects associated with cisplatin and its congeners. Further pressing problems are inherent or acquired platinum resistance and narrow limitations in the profile of responding cancers. For example, the prototypical cisplatin is particularly curative in the case of testicular cancer with a cure rate of up to 95%. However, for about 5% of the patients, the cancer shows no response to the treatment, attributed to an inherent and not yet fully understood platinum resistance. Even for those patients who respond to the initial treatment, a recurring cancer may not react to subsequent treatment due to acquired platinum resistance. Unfortunately, for some major cancers such as lung, breast, and head cancers, therapy with the current platinum drugs is not curative. Oxaliplatin appears to be particularly potent for colon cancer and is the treatment of choice for tumors that prove to be resistant to cisplatin or carboplatin by virtue of the different structural demand of the *trans*-(*R*,*R*)-1,2-diaminocyclohexane ligand.

In the quest to overcome the problems associated with cisplatin-based therapy, countless platinum complexes have been tested for their cytostatic activity. On the basis of such empirical studies, structure−activity rules (SARs) have been established and were first formulated by Cleare and Hoeschele.[4] According to SARs, activity is generally found for platinum(II) complexes that are neutral and planar and adhere to the general formula *cis*-$Pt^{II}A_2X_2$, in which A represents a neutral amine ligand bearing 1−3 protons. X or X_2 represents an anionic leaving group such as halide, oxalate, and malonate, which allows slow hydrolysis. Platinum compounds that conform to these rules are considered as "classical" or "traditional" platinum cytostatics.

A series of essential properties are accredited to the amine ligand, which is assumed to remain coordinated during the whole action time of the drug. First, the amine appears to function as a "carrier ligand" for transport of the drug from the bloodstream through the cell membrane of the cancer cells. The amine is thought to identify cancer cells by preferably penetrating the membranes of certain cancer cells and sparing the healthy tissue. This feature allows the drug to accumulate in the cancer cells, minimizing side effects. In order to optimally penetrate the lipophilic cell membrane, the drug molecule must be neutral and sufficiently lipophilic but not exceedingly bulky. In this way, the "carrier ligand" should provide a route to enlargement of the so-far-rather-limited scope of treatable

Received: July 14, 2016

DOI: 10.1021/acs.inorgchem.6b01690
Inorg. Chem. XXXX, XXX, XXX−XXX

cancers. Second, once inside the cancer cells, the drug molecule must be able to move through the cell fluid with its countless ingredients and find its way to bind selectively to DNA. Migration to and along DNA with selection of the DNA purine bases for coordination occurs by reversible hydrogen bonding of the N−H functions, which therefore appear indispensable. While the anionic ligands are cleaved off by hydrolysis, the remaining aminoplatinum(II) species latches onto the DNA and causes its denaturation.[5] Third, coordination of the amine ligand to both platinum and the purine bases must be strong enough to hold platinum at its ultimate position, avoiding efflux from the cell by reverse migration. Finally, as DNA repair mechanisms responsible for "Pt resistance" come into action, these therapy-counteracting mechanisms cope most efficiently with the small $(H_3N)_2Pt^{II}$ moiety of cisplatin and carboplatin, which therefore cannot prevent "Pt resistance". Aminoplatinum(II) moieties of disk shape and larger bulk, as is the case for oxaliplatin, appear to withstand such mechanisms more effectively and therefore appear to thwart an upcoming "Pt resistance".

According to the SARs, platinum complexes bearing secondary amines, which are usually sterically more demanding, are expected to be less potent than those with ammine or primary amines. However, because the traditional platinum cytostatics do not appear to provide a remedy for the adverse effects and limitations of the current platinum-based treatments, current research focus is set on "non-traditional" platinum drugs, molecules that are not necessarily consistent with SARs.[6] So far, little attention has been given to the intermolecular hydrogen bonding extended by the carrier ligands by self-association of the complexes and to water.[7]

Some years ago, we studied complexes of nickel(0) with 3,7-dimethylbispidine (bispidine = 3,7-diazabicyclo[3.3.1]-nonane).[8] The unexpected stability of these complexes, which runs contrary to the hard and soft acids and bases concept, can be explained by the principles of preorganization (ligand) and prepositioning (ligand atoms) as the essential features of the macrocyclic effect.[9] The bispidine−metal entity comprises an adamantane-type structural unit, featuring four six-membered rings. We note that many herbal alkaloids [(−)-sparteine, (+)-lupanine, (−)-cytisine, etc.] contain such a bispidine core. The relevance of the bispidine scaffold in biologically active systems is well documented.[10] Such considerations raised the question of whether simple bispidines, unsubstituted at both N atoms, could provide useful "carrier ligands" for platinum cytostatics.

On the basis of an improved synthesis of the parent bispidine ($C_7H_{12}(NH)_2$, **A**)[11,12] and knowledge of its properties so gained,[13] we recently synthesized the series of cisplatin, carboplatin, and oxaliplatin analogues **A1**−**A3** (Chart 2).[14] Similarly, in a subsequent series, the 9,9-dihydroxy-substituted derivatives **B1**−**B3** were prepared.[15]

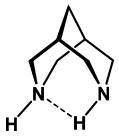

A

The cytotoxic potency of these compounds has been tested against the ovarian cancer line A2780, the cisplatin-resistant subline A2780 CisR, and the leukemia cell line K562. While a general decrease of the cytotoxic potency was noted compared to that of the reference compounds, the complexes still retained potency on the micromolar concentration level. Particular potency was found with respect to A2780 CisR, suggesting that overcoming "Pt resistance" might be a possible feature.

Chart 2. Bispidine-Type Modified Analogues of Cisplatin, Carboplatin, and Oxaliplatin

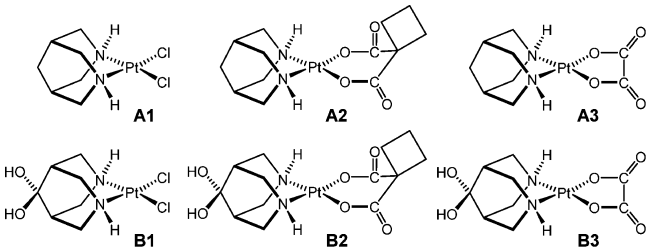

In a continuation of these studies, we became interested in what effect might follow from the incorporation of oxygen in the bispidine skeleton, as is the case for 9-oxabispidine (**C**). The bridging O atom was expected to result in a balancing of the hydrophilicity and lipophilicity and, at the same time, to reduce the size of the bispidine ligand by virtue of the short C−O bonds. It was considered an open question as to how the additional basic sites of the O atom would alter the properties of (bispidine)platinum(II)-type complexes.

We therefore revisited the previous synthesis of **C** by Stetter and Meissner, prepared and characterized complexes **C1**−**C3** as the **C** derivatives of cisplatin, carboplatin, and oxaliplatin, and probed their cytotoxic potency (Chart 3). A subsequent paper will deal with related complexes of 9,9-difluorobispidine (complexes **D1**−**D3**).[16]

Chart 3. New (9-Oxabispidine)platinum(II) Complexes

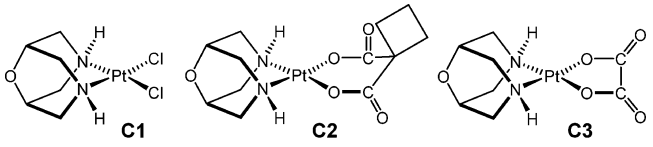

2. RESULTS AND DISCUSSION

Synthesis and Properties of 9-Oxabispidine (C). The synthesis of **C** was performed by modification of the route outlined by Stetter and Meissner (Scheme 1; retained notation).[17] After protection of the N atom in diallylamine by phenylsulfonate to obtain **I**, the C═C bonds were

Scheme 1. Synthesis of C (after Stetter and Meissner)

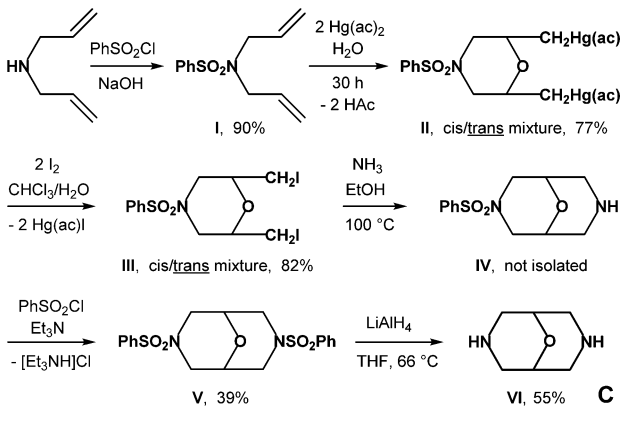

C

DOI: 10.1021/acs.inorgchem.6b01690
Inorg. Chem. XXXX, XXX, XXX−XXX

oxygenated with mercury diacetate/water to give a cis/trans mixture of mercuric morpholine (**II**), which was converted to the iodide **III**. Ring closure with ammonia afforded (non-isolated) 3-(phenylsulfonyl)-9-oxabispidine (**IV**), which in a pyridine solution was converted to crystalline 3,7-bis-(phenylsulfonyl)-9-oxabispidine (**V**). Final cleavage of the protection groups with $LiAlH_4$ afforded 9-oxabispidine (**VI**, denoted as **C** in this paper).

We encountered several pitfalls during the synthesis of **C**, which call for special attention. (i) Stetter and Meissner anticipated that during the formation of the morpholine intermediates **II** and **III** the cis isomers would prevail. We found, however, while investigating the iodide **III** by NMR, that **cis-III** is actually the minor isomer in the reaction mixture, with the cis/trans ratio being as low as 1:2. From the oily raw product, large chunks of **cis/trans-III** can be crystallized. Repeated recrystallization from ethanol leads to extraction of pure **trans-III** and enrichment of **cis-III** in the mother liquor. Both isomers have been characterized by their NMR spectra, and the structure of **trans-III** has been established by single-crystal X-ray structure analysis (Table S1 and Figure S1 in the Supporting Information, SI). The crude **cis/trans-III** can be used for further reactions. (ii) Carrying out step **IV** → **V** in pyridine did not produce pure **V** but the pyridine solute **V**·$^1/_2$**py** as a crystalline product. We have verified the identity of **V**·$^1/_2$**py** by X-ray structure analysis (see below). The thermal effect reported to occur at 150 °C appears to be caused by the elimination of solute pyridine rather than devitrification ("Kristallumwandlung"),[17] which we were able to rule out for pyridine-free **V**. The presence of pyridine complicated the next reaction step because it results in $[C_5H_5NH]Cl$ as a byproduct, which is tedious to remove. We were able to avoid this problem by carrying out step **IV** → **V** in a tetrahydrofuran (THF) solution. Nevertheless, NEt_3 was necessary as a base, which afforded $[Et_3NH]Cl$. The latter was effectively removed by aqueous KOH to yield pure **V**. (iii) We recommend that the reduction **V** → **VI** be carried out with freshly recrystallized (colorless) $LiAlH_4$, which markedly increases the yield. (iv) Quenching the reaction mixture with methanol (MeOH) instead of water allowed direct sublimation of the strongly hygroscopic **VI** ($OC_6H_{10}(NH)_2$, **C**) from the reaction mixture, thus avoiding tedious workup. The full protocol of the modified synthesis, including the NMR characterization of intermediate **cis/trans-III**, is described in the SI (Figures S2–S5).

The melting point of **C** is 76 °C and thus much lower than that of parent **A** (198 °C).[13] A differential scanning calorimetry (DSC) investigation rules out any phase transition prior to melting for the ordered-crystalline **C**, whereas the parent **A** seems to transform into a dynamically disordered phase. Similar to **A**, solid **C** sublimes under vacuum before melting. It dissolves well in pentane at ambient temperature, from which it can be recrystallized at 0 °C. The compound has a particularly unpleasant and characteristic odor when finely divided. The odor is also noticeable for its solutions in THF, acetone, and water but is substantially reduced in solutions of *N*,*N*-dimethylformamide (DMF) and dimethyl sulfoxide (DMSO) (hardly noticeable). This fact may be explained by the effective hydrogen bonding of the NH protons to the increasingly basic O of the latter solvents. Solid **C** is strongly hygroscopic and liquefies within minutes when exposed to air.

The electron impact mass spectrometry spectrum (25 °C) of **C** was recorded by means of gas chromatography–mass spectrometry (GC–MS) coupling because of the high vapor pressure of the compound. Fragmentation of the molecular ion $[M]^+$ (*m*/*e* 128, 48%) occurs in a fashion similar to that of parent **A**,[12] in that the initial ionization at N is followed by 2-fold α-C–C bond cleavage[18] and two proton-transfer steps to afford, inter alia, the 2,3-dehydromorpholinium cation $[C_4H_6NO]^+$ (*m*/*e* 84) as a prominent ion (eq 1). Moreover,

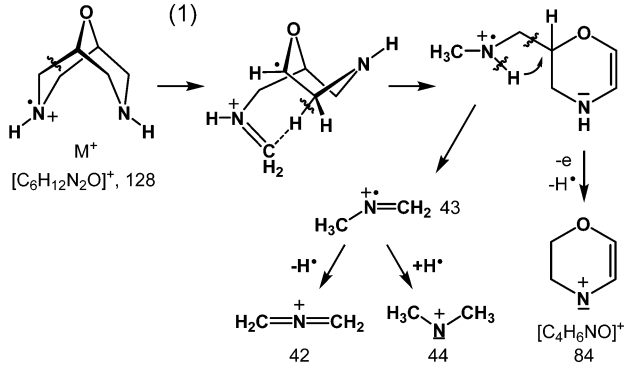

electrospray ionization mass spectrometry in positive operation mode (ESI^+ MS) of a solution of **C** in MeOH shows $[M + H]^+$ as the sole cation. Keeping a solution of **C** in CH_3OD for 2 days resulted in H/D exchange at NH with the formation of $OC_6H_{10}(ND)_2$ (**C**-d_2), which was isolated by vacuum evaporation of the solvent below 0 °C. The IR spectra of **C** and **C**-d_2 (see the SI) are described below, together with those of complexes **C1**–**C3**.

The ^{1}H NMR spectrum (THF-d_8) of **C** shows for the bridgehead OCH [δ(H) 3.23; ^3J = 3.6 Hz] a triplet because of coupling to two NCH_{ax}. The OCH signal occurs expectedly at low field due to the neighboring O atom, in contrast to the situation observed for parent **A** [δ(H) 1.45].[13] $NCH_{eq}H_{ax}$ gives rise to AB-type signals with typical geminal coupling. The higher field doublet [δ(H) 2.84, ^2J = 12 Hz] lacks further visible coupling and can be assigned to NCH_{eq}, while the lower field signal for NCH_{ax} is a doublet of doublets [δ(H) 3.13, ^2J = 12 Hz, ^3J = 3.6 Hz] due to coupling with the bridgehead OCH. Intriguingly, in **C**, the signal of NCH_{ax} is shifted downfield and that of NCH_{eq} upfield so that the order of the signals is reversed compared to that of **A** (it is again reversed for complexes **C1** and **C2**; see below).[19] The assignment of the $NCH_{eq}H_{ax}$ signals of **A** and **C** ensues from correlation of the dihedral angles with H2/5 (see the molecular structures) and the coupling constants according to the Karplus equation. Because of flattening of the chair conformation of the six-membered rings at N, the dihedral angle between CH2/5 and NCH_{ax} (54°) is relatively small, and the corresponding ^3J coupling is larger and hence resolved. This relationship is different for NCH_{eq} (64°, $^3J \leq 2$ Hz).

The NH signal at δ(H) 2.34 ($w_{1/2}$ = 1.7 Hz) occurs at lower field than that for **A** [δ(H) 2.10]. The NH signal is markedly broadened at −80 °C [δ(H) 2.61, $w_{1/2}$ = 22 Hz], which is explained by the slow exchange of the bonding situations of the *endo*- and *exo*-NH protons according to eq 2.

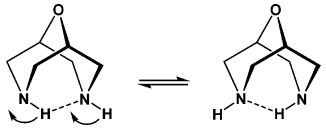

^{13}C NMR displays for **C** merely two sharp signals in the 1:2 intensity ratio [δ(C) 66.8 (OCH), 47.5 (NCH_2); δ(C) 28.9 (CH), 52.1 (NCH_2) for **A**].

DOI: 10.1021/acs.inorgchem.6b01690
Inorg. Chem. XXXX, XXX, XXX–XXX

When **C** is dissolved in CH_2Cl_2, it slowly reacts with the solvent by nucleophilic displacement of Cl by N to eventually (after several days) give pure 1,3-diaza-6-oxaadamantane dihydrochloride $[OC_7H_{12}N_2(HCl)_2$, **VII-2HCl**; eq 3]. This

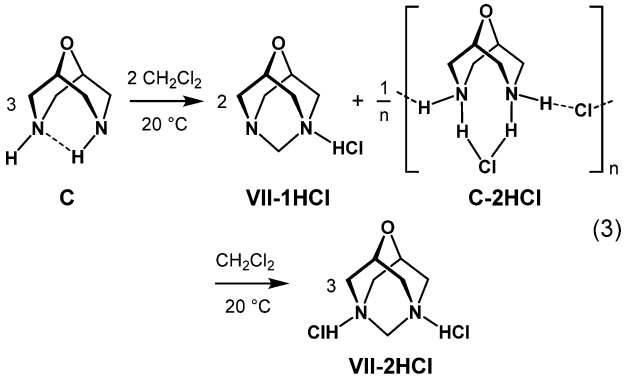

deceptively simple reaction proceeds in a multistage cascading fashion because of the action of alternating bases. The stepwise nature of the reaction is clearly apparent by the formation of colorless needles of 9-oxabispidine dihydrochloride $[OC_6H_{10}(NH)_2(HCl)_2$, **C-2HCl**], within 1 day, which redissolve to be replaced by the colorless precipitate of **VII-2HCl**. The reaction is analogous to that of **A** with CH_2Cl_2, which comes to a halt at the stage of the insoluble bispidine dihydrochloride (**A-2HCl**).[13] However, because the 9-oxabispidine analogue **C-2HCl** is moderately soluble in CH_2Cl_2, this intermediate reacts further with full conversion of the initial **C** into **VII-2HCl**.

When the reaction of eq 3 by ^{1}H NMR for a solution of **C** in CD_2Cl_2 is monitored, reaction steps a–d can be distinguished depending on the base in action (Scheme 2).[13] In the first step (a), attack of **C** on CH_2Cl_2 (CD_2Cl_2) formally generates **VII-2HCl**, which in the presence of **C** immediately becomes fully deprotonated, forming 1,3-diaza-6-oxaadamantane (**VII**) and soluble **C-1HCl**. This step takes about 12–24 h and is distinctly slower than the analogous reaction of **A** with CH_2Cl_2 (E = CH_2; 90 min). The lower reactivity of **C** compared to that of **A** is consistent with the electron-withdrawing effect of O, which reduces the nucleophilicity of the N atoms while increasing the acidity of the NH protons. In the course of step a, the NMR signals of **C**/**C-1HCl** (in rapid exchange) move to lower field due to an increasing amount of **C-1HCl**, and the new signals of **VII** arise at constant chemical shifts.

When all **C** is consumed (mostly in its function as a base), the generated **C-1HCl** undergoes a similar but still slower reaction (steps b and c). In step b, 0.5 equiv of **C-1HCl** reacts with 0.5 equiv of CH_2Cl_2, and all of intermediate **VII** serves as a base to give **VII-1HCl**. During this step, the NMR signals of **VII**/**VII-1HCl** (in rapid exchange) shift to lower field, while the signals of **C-1HCl** retain their chemical shifts but decrease in intensity. In step c, when all of **VII** is consumed, a further 0.5 equiv of **C-1HCl** reacts with 0.5 equiv of CH_2Cl_2, with **C-1HCl** acting as base to partially deprotonate intermediate **VII-2HCl**, producing a further 0.5 equiv of **VII-1HCl**. The concomitantly formed **C-2HCl** associates to give polymeric chains and so precipitates from the solution. In this step, the signals of **VII-**

Scheme 2. Generalized Stepwise Reaction of Bispidines with CH_2Cl_2 To Give 1,3-Adamantane Derivatives [for C, E = Oxygen]

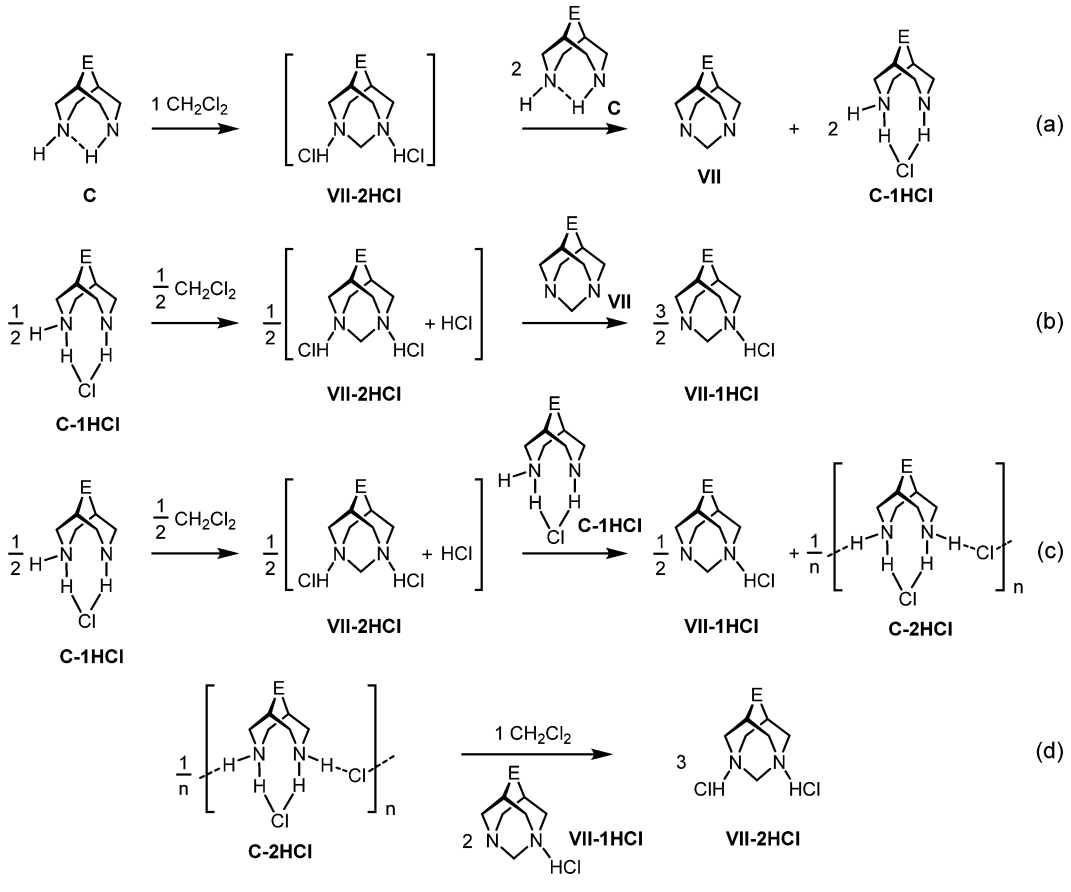

DOI: 10.1021/acs.inorgchem.6b01690
Inorg. Chem. XXXX, XXX, XXX–XXX

Table 1. Crystal Data for $V^{\cdot 1}/_2$py, C, C1, and C2

	$V^{\cdot 1}/_2$py	C	C1	C2
internal identification	8721	8789	9221	8865
CCDC no.	1491344	1491345	1491346	1491347
empirical formula	$C_{18}H_{20}N_2O_5S_2{}^{\cdot 1}/_2C_5H_5N$	$C_6H_{12}N_2O$	$C_6H_{12}Cl_2N_2OPt$	$C_{12}H_{28}N_2O_{10}Pt$
color	colorless	colorless	colorless	colorless
fw (g mol^{-1})	448.03	128.18	394.17	555.45
temp (K)	100(2)	100(2)	100(2)	100(2)
wavelength (Å)	1.54178	0.71073	0.71073	0.71073
cryst syst	monoclinic	monoclinic	orthorhombic	triclinic
space group	$P2_1/n$ (No. 14)	$P2_1/c$ (No. 14)	$Pnma$ (No. 62)	$P\bar{1}$ (No. 2)
unit cell dimens				
a (Å)	9.7890(6)	6.3990(17)	9.074(3)	9.2354(19)
b (Å)	16.0478(10)	9.167(2)	9.0848(9)	12.847(3)
c (Å)	12.7315(8)	11.334(3)	11.483(3)	17.067(4)
α (deg)	90.0	90.0	90.0	69.229(3)
β (deg)	96.1711(15)	95.314(5)	90.0	89.034(3)
γ (deg)	90.0	90.0	90.0	78.774(3)
V (Å^3)	1988.4(2)	662.0(3)	946.6(4)	1854.2(7)
Z	4	4	4	4
V/Z (Å^3)	497.1	165.5	236.7	463.6
calcd density (Mg m^{-3})	1.497	1.286	2.766	1.990
abs coeff (mm^{-1})	2.766	0.090	15.341	7.619
F(000)	940	280	728	1088
cryst size (mm^3)	0.49 × 0.29 × 0.16	0.42 × 0.29 × 0.04	0.11 × 0.06 × 0.05	0.39 × 0.27 × 0.11
θ range for data collecn (deg)	4.449−67.640	2.863−33.727	2.859−35.984	2.522−28.280
index ranges	$-11 \le h \le 11$, $-19 \le k \le 19$, $-15 \le l \le 15$	$-9 \le h \le 9$, $-14 \le k \le 13$, $-17 \le l \le 17$	$-14 \le h \le 14$, $-15 \le k \le 15$, $-18 \le l \le 18$	$-12 \le h \le 12$, $-17 \le k \le 17$, $-22 \le l \le 22$
no. of rflns collected	87888	21667	31678	44173
no. of indep rflns	3574 (R_{int} = 0.0368)	2645 (R_{int} = 0.0907)	2288 (R_{int} = 0.0259)	9197 (R_{int} = 0.0492)
no. of rflns with $I > 2\sigma(I)$	3561	1938	2275	8384
completeness (%)	99.3 (θ = 67.679°)	100.0 (θ = 25.242°)	93.9 (θ = 25.242°)	99.9 (θ = 25.242°)
abs corrn	Gaussian	Gaussian	Gaussian	Gaussian
max/min transmn	0.72113/0.35454	0.99599/0.96575	0.52144/0.22697	0.42254/0.13855
full-matrix least squares	F^2	F^2	F^2	F^2
no. of data/restraints/param	3574/0/271	2645/0/90	2288/0/70	9197/12/539
GOF on F^2	1.059	1.175	1.178	1.028
final R indices [$I > 2\sigma(I)$]				
R1	0.0285	0.0780	0.0127	0.0227
wR2	0.0744	0.2146	0.0309	0.0549
R indices (all data)				
R1	0.0286	0.1098	0.0128	0.0261
wR2	0.0745	0.2276	0.0309	0.0568
largest diff peak/hole (e Å^{-3})	0.296/−0.455	0.621/−0.385	1.563/−1.231	1.696/−2.341

1HCl increase in their relative intensity with retained chemical shifts and the signals of **C-1HCl** largely disappear from the spectrum. In the last step (d), solid **C-2HCl** redissolves to similarly react with CH_2Cl_2, and all of **VII-1HCl** acts as a base, affording the complete formation of **VII-2HCl**. During this step, the NMR signals of **VII-1HCl/VII-2HCl** shift further to lower field until the spectrum of **VII-2HCl** is reached. Thus, in steps a−c, **VII-2HCl** is a transient intermediate but eventually reappears as the product in step d. Four different bases come into action and are consumed in the various steps.

Crystal and Molecular Structure of $OC_6H_{10}(NSO_2Ph)_2{}^{\cdot 1}/_2$py ($V^{\cdot 1}/_2$py). The isolated crystalline intermediate **V** persistently contained pyridine. In order to clarify the nature of the compound, we carried out an X-ray structure analysis. Details of the structure analysis are given in Table 1, and a drawing of the compound is shown in Figure 1.

3,7-Bis(phenylsulfonyl)-9-oxabispidine crystallizes from pyridine in the monoclinic crystal system, space group $P2_1/n$ (No. 14), together with half a pyridine molecule, hence **$V^{\cdot 1}/_2$py**. There are four identical asymmetric 3,7-bis(phenylsulfonyl)-9-oxabispidines (**V**) and two pyridine molecules in the unit cell. The two pyridine molecules reside on inversion centers located at $b/2$ and the center of the ac plane. Owing to the positions of the solute pyridine molecules about inversion centers, the

DOI: 10.1021/acs.inorgchem.6b01690
Inorg. Chem. XXXX, XXX, XXX−XXX

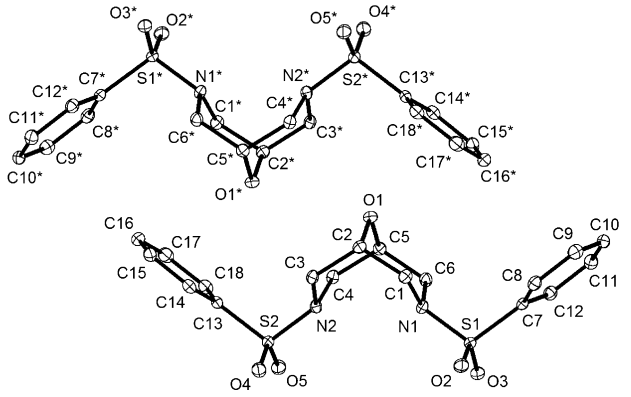

Figure 1. Molecular structure of $\mathbf{V}\cdot{}^{1}/_{2}\mathbf{py}$ (pyridine molecules and H atoms are omitted). Shown are two identical molecules of **V**, related by an inversion center. Selected bond distances (Å), nonbonding distances (Å), and bond angle (deg): O1−C2 = 1.4319(2), O1−C5 = 1.4352(2), C2···C5 = 2.336(2), N1···N2 = 2.968(2), O1···O1* = 3.423(2); C2−O1−C5 = 109.1(1).

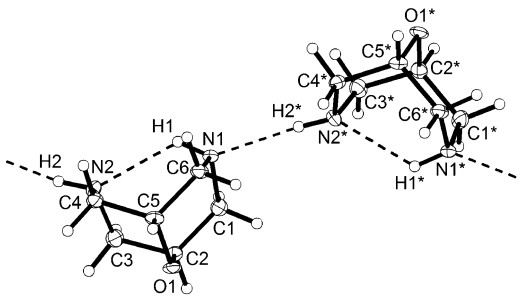

Figure 2. Molecular structure of **C** in the crystal, showing two consecutive molecules of opposite environmental chirality in a chain and the intramolecular and intermolecular hydrogen-bonding interactions. Selected distances (Å) and angles (deg): N1−H1 = 0.88(4), N2···H1 = 2.28(4), N2−H2 = 0.88(4), N1···H2* = 2.19(4), N1···N2 = 2.88(4), N1···N2* (intermolecular) = 3.055(3), C2···C5 = 2.344(3); C2−O1−C5 = 109.0(2), N1−H1···N2 = 125(2), N2−H2···N1* = 169(2).

isoelectronic N3 and the C20H20 entities of the pyridine molecules are disordered in a 1:1 ratio.

Both morpholine rings of the **C** skeleton adopt a slightly flattened chair conformation, resulting in a relatively large intramolecular N1···N2 distance of 2.968(2) Å. The two $PhSO_2$ substituents at N1 and N2 formally occupy equatorial (exo) positions in the six-membered oxa rings, which leaves the electron pairs in axial (endo) positions, pointing toward one another. Because the orientation of the phenyl substituents is antiperiplanar to the N lone pairs, as is typical for this structural entity,[20] the molecules assume a W-shaped conformation of which the three top tips are given by the central O1 bridge and *p*-CH of the flanking phenyl rings, whereas the two bottom tips can be represented by S1O2O3 and S2O3O4.

Around the center and origin (viz. corners) of the unit cell, each two nonsymmetric molecules form an inversion-related racemic pair by mutual alignment of the W top tips [the intermolecular O1···O1* distance is 3.423(2) Å]. Such pairs are related to one another by the four 2-fold screw axes parallel to *b*; the same holds for the pyridine molecules at different positions. Because there is no $\pi-\pi$ stacking in the structure, the pyridine molecules appear to fill the voids in the lattice of **V**.

Crystal and Molecular Structure of 9-Oxabispidine (C). Single crystals of **C** were obtained by sublimation. **C** crystallizes in the monoclinic space group $P2_1/c$ (No. 14), different from that of the parent bispidine **A** (Figure 2).[13,21] We will show later that 9,9-difluorbispidine (**D**)[16] crystallizes in the same space group as that for **C**. The unit cell of **C** contains four equivalent asymmetric molecules, which pairwise belong to two chains created by N−H···N hydrogen bonding. The NH H atoms were located on a difference Fourier synthesis and refined with the isotropic atomic displacement parameter; nevertheless, the relatively high *R* indices of the structure solution indicate that the positions of the H atoms should be treated with caution and are therefore not discussed in detail.

Similar to the situation in **A**, **C** exhibits a chair−chair conformation of the two morpholine rings, with the N1−H1 proton in an endo orientation and the N2−H2 proton in an exo orientation with respect to the core of the molecule. N1−H1 forms an intramolecular hydrogen bond, N1−H1···N2, with a (nonbonding) N1···N2 distance of 2.875(3) Å, which is slightly longer than those in **A** [2.849(2) Å] and **D** [2.830(2) Å]. Within the morpholine rings in **C**, the C−O bonds at 1.44 Å (mean) are much shorter than their geometric C−C bond equivalent (1.53 Å, mean) in **A** and are even shorter than N−C (1.47 Å, mean). As a consequence of the oxygen tie, the (nonbonding) C2···C5 distance reflecting the "thickness" of the molecule is reduced to 2.344(3) Å in **C** [from 2.462(2) Å in **A** and 2.435(3) Å in **D**] and is now distinctly shorter than the C1···C6 and C3···C4 distances at 2.41 Å (mean). This results in a "squeezed" and concave geometry of the **C** skeleton, together with a widened N1···N2 bite.

The C2−O1−C5 [109.0(2)°] and C−N−C [110.2(4)°, mean] angles in **C** are closer to the tetrahedral ideal than the corresponding angles in **A** (C2−C7−C5 107.4° and C−N−C 112.0°, mean). While the chair conformation of the morpholine ring involving N2 is close to what is expected (dihedral angles 55−63°), that of the ring involving N1 is flattened at N1 (dihedral angles 47−64°), which appears to result from the intramolecular N1−H1···N2 hydrogen bridge, similar to the situation in **A**.

In the crystal, the asymmetric molecules are head−tail associated with alternating chirality, albeit weakly manifested, and arranged to both sides of a glide plane (parallel to *ac*), forming chains that extend along the *c* axis. Association is given by intermolecular N2−H2···N1* hydrogen bonds [H2···N1* 2.19(4) Å and N2−H2···N1* 169(2)°]. The short intermolecular N2···N1* distance at 3.055(3) Å [**A**, 3.114(2) Å; **D**, 3.192(2) Å] suggests relatively strong hydrogen bonding, indicating an increased acidity of the NH protons. Interestingly, the ethereal O1 is not involved in any N−H···O bonding, which appears to be in agreement with the concept of Etter[22] that in complex systems the strongest hydrogen-bond donor (NH) will interact with the strongest base, viz., the secondary amine.

Such chains are piled up along the *b* axis, forming pads extending parallel to the *bc* plane. Neighboring chains run in the opposite direction. Molecules that are "atop" one another are related by a 2-fold screw axis parallel to *b*, and these molecules interact by a hydrogen-bonding interaction, N2C4−H4B···O1* 2.61(4) Å [145(2)°], involving one NCH_{eq} proton (out of four) and the ethereal O atom of the adjacent chain. These C−H···O bonds appear slightly shorter than the sum of the Bondi van der Waals (vdW) radii of H (1.20 Å)[23a] and O (1.52 Å).[23]

DOI: 10.1021/acs.inorgchem.6b01690
Inorg. Chem. XXXX, XXX, XXX−XXX

There is a discernible decrease in the molecular volume upon going from parent bispidine **A** (180.2 Å^3 at 200 K) to **C** (165.5 Å^3 at 100 K; $\Delta V_m = -14.7$ Å^3), which exceeds that calculated ($\Delta V_{calc} = -12.64$ Å^3) for the replacement of CH_2 by O based on the Hofmann atom volume increments [V(C) = 13.87 Å^3, V(H) = 5.08 Å^3, and V(O) = 11.39 Å^3],[24] thus indicating an overall tighter packing of the molecules in **C**.

Synthesis of the (9-Oxabispidine)platinum Complexes C1−C3. The synthesis of the (9-oxabispidine)platinum complexes largely followed that of the parent bispidine complexes **A1**−**A3**.[14] Thus, (1,5-hexadiene)platinum dichloride[25] was reacted with 1 equiv of **C** in DMF at 65 °C to afford a yellow precipitate of $\{OC_6H_{10}(NH)_2\}PtCl_2$ (**C1**; Scheme 3).

Scheme 3

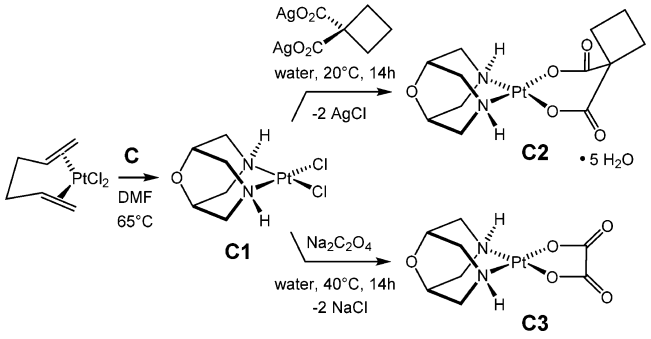

The isolated **C1** was then further reacted with Ag_2(cbdca) in water to obtain, after removal of AgCl, an aqueous solution of $\{OC_6H_{10}(NH)_2\}Pt\{(O_2C)_2C_4H_6\}\cdot 5H_2O$ (**C2**), which was isolated after concentration. Complex **C2** crystallizes from water as a pentahydrate but largely loses the water under vacuum. The reaction of **C1** with sodium oxalate in water afforded $\{OC_6H_{10}(NH)_2\}Pt(C_2O_4)$ (**C3**) as an off-white precipitate.

The dichloride **C1** is practically insoluble in DMF (from which it is obtained during the synthesis) and dissolves only scarcely in water, even when heated. We will show below that the molecules of **C1** form a planar 2D network in the crystal by intermolecular N1−H1···O1 and N2−H2···Cl2 hydrogen bonding, and these bonds are apparently not readily cleaved by water. When forced to dissolve in hot water (D_2O), a series of species is formed according to NMR, which suggests partial or full hydrolysis, as depicted in eq 4.

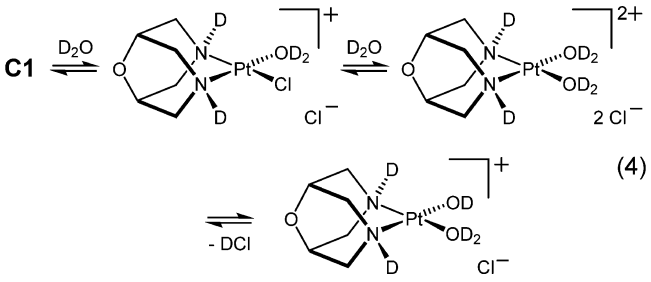

(4)

Compound **C1** dissolves slowly in DMSO (DMSO-d_6) at ambient temperature, but dissolution may be spurred on by sonication. In the ^{1}H and ^{13}C NMR spectra (see below) of such a solution, in addition to the signals of the C_{2v}-symmetrical **C1** (33%), the signals of the ionic **C1-DMSO** (67%) of lower symmetry are observed, demonstrating displacement of one chloride by DMSO in an equilibrium reaction (eq 5).

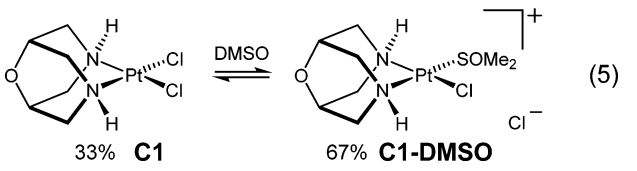

(5)

Displacement reactions at platinum(II) by DMSO have been studied before.[14,15,26,27] The mutual Cl^-/DMSO replacement reactions of eq 5 are slow, as evidenced by the sharp NMR signals for **C1** and **C1-DMSO**. In contrast, exchange of the DMSO ligand in **C1-DMSO** with the solvent appears to be fast because no separate ^{1}H and ^{13}C NMR signals were found for the coordinated DMSO. The presence of the cation $[\{OC_6H_{10}(NH)_2\}PtCl(DMSO)]^+$ (m/e 436) was verified by ESI MS. No dication $[\{OC_6H_{10}(NH)_2\}Pt(DMSO)_2]^{2+}$ was detected by either NMR or ESI MS. DMSO solutions of **C1** can be diluted with water.

Unlike **C1**, the cbdca derivative **C2** is quite soluble in water, from which it forms the pentahydrate. After removal of water under vacuum, the complex still dissolves in DMSO and DMF but not in acetone or THF. The relatively high solubility of **C2** can be attributed to its "nutshell" structure, which appears to impede association with neighboring molecules by strong hydrogen bonds.

The clearly more planar oxalate **C3** is again virtually insoluble in all solvents including DMSO and DMF, also when heated. Thus far, we have been unable to obtain crystals suitable for X-ray structure analysis. Taking into account various forms of N−H···O bonding, we assume that **C3** adopts a polymeric planar chain structure like **A3**[14] or a planar 2D network structure similar to that of **C1**. The addition of oxalic acid to a suspension of **C3** in water appears to increase its solubility.

All of the platinum complexes are odorless, despite the intense odor of the free **C**. The complexes (**C2** after dehydration) are thermally extraordinarily stable up to about 320 °C, and no change in the appearance was noticed. No thermal effect was detected by DSC below this temperature. The $[M + Na]^+$ ions were observed in the ESI MS spectra of solutions of the complexes in MeOH, recorded in a positive operation mode.

IR Spectra of C, C-d_2, and C1−C3. The IR spectra of the compounds are included in the SI (Figures S12−S16). The spectra of **C** and **C-d_2** may be compared with the spectra of the other isolated N-unsubstituted bispidines **A**[13] and **D**,[16] and the spectra of **C1**−**C3** to those of **A1**−**A3**,[14] **B1**−**B3**,[15] and **D1**−**D3**.[16] The extraordinary hygroscopy of **A** and **C** may have resulted in incidental uptake of some moisture during recording of the spectra. Some residual water is also contained in the pentahydrate **C2** after drying under vacuum. The spectra of the malonate **C2** and oxalate **C3** are dominated by very strong bands due to carbonyl stretching (1700−1600 cm^{-1}) and ν(C−O/C−C) coupling vibrations (1400−1300 cm^{-1}). The assignment of the IR bands was made by a comparison with the literature values.[28]

While **A** and **D** exhibit relatively small ν(NH) vibrational humps in the 3320−3260 cm^{-1} region, **C** features a prominent ν(NH) band at 3213 cm^{-1}. For **C-d_2**, this band is shifted to the 2400 cm^{-1} region and is multifold split. Because **C** and the 9,9-difluorinated **D** are exempt from containing bridging 9-CH_2 and because $\nu(C_{tert}H)$ is usually weak, the bands at 2916 and 2820 cm^{-1} can be safely attributed to $\nu_{as}(CH_2)$ and $\nu_s(CH_2)$ of NCH_2. The weak bands at 2800−2700 cm^{-1} can be considered

DOI: 10.1021/acs.inorgchem.6b01690
Inorg. Chem. XXXX, XXX, XXX−XXX

to be $\nu(NCH_{ax})$ Bohlmann bands.[29] A series of bands at 1500−1200 cm^{-1} are attributed to $\delta(CH_2)$ and $\delta(CH)$ bending vibrations. All CH ν and δ bands remain unaltered for **C-d_2**.

Most bands of **C** in the 1200−450 cm^{-1} region are shifted to lower wavelengths for **C-d_2** and gain sharpness, suggesting the occurrence of NH (respectively ND)-coupled vibrations. Upon going from **C** to **C1**−**C3**, the ν(NH) bands are shifted to 3200−3100 cm^{-1}. No Bohlmann bands $\nu(NCH_{ax}) \leq 2850$ cm^{-1} are visible because the lone electron pairs at N, now binding to Pt^{II}, are no longer free. For **C** and **C1**−**C3**, we find sharp bands of medium intensity at 1160−1100 cm^{-1} assigned to ν_{as}(C−O−C) and a further sharp band at 980−960 cm^{-1} assigned to ν_s(C−O−C) of the oxygen bridge. While the uncoordinated **C** exhibits a very strong *broad* band at 880−780 cm^{-1} (centered at 828 cm^{-1}), **C1**−**C3** agree in a very strong *sharp* band at 860 cm^{-1}. These bands appear unique and characteristic for the **C**-derived compounds, and we attribute them to δ_{as}(C−O−C) bending of the **C** skeleton. While the skeleton of the uncoordinated **C** still exhibits slight flexibility, which includes chair−boat conformational changes and entails lower-energy vibrations and a broader distribution profile, the adamantane-type structures of complexes **C1**−**C3** are fully rigid, accounting for higher energy and sharper $\nu_{as/s}$(C−O−C) vibrations.

NMR Spectra of C1 and C2. Because of the low solubility, ^{1}H and ^{13}C NMR spectra were recorded only for solutions of **C1** in DMSO-d_6 and **C2** in DMSO-d_6 and D_2O. We describe first the spectra of **C2**.

The ^{13}C NMR spectra of **C2** in DMSO-d_6 and D_2O are inconspicuous and feature six singlets. The ^{1}H NMR spectrum of **C2** in DMSO-d_6 is somewhat broadened. The NH signal at δ(H) 7.48 is flanked in the 300 MHz spectrum by a pair of humps, but these vanish at 600 MHz (Figure S10) and thus appear to be due to the ^{14}N quadrupole. Compared to uncoordinated **C** (solvent of THF-d_8), all **C** signals are shifted to lower field, and the order of the $NCH_{eq}H_{ax}$ signals is reversed so that the NCH_{ax} signal is now at higher field. The ^{1}H NMR spectrum of **C2** in D_2O is much better resolved (Figure S11), although here no NH signal is found, owing to H/D exchange. The other **C** signals are shifted to still lower field. The signal of NCH_{eq} is a doublet [δ(H) 3.51; ^2J(HH) = 13.1 Hz] because of the geminal coupling and small vicinal coupling [^3J(HH) ≤ 2 Hz] ensuing from the large torsional angle with OCH (63.0°, mean; see the X-ray structure). The higher field signal for NCH_{ax} [δ(H) 3.37; ^2J(HH) = 13.1 Hz; ^3J(HH) = 3.5 Hz] shows additional fine splitting by coupling with OCH, in agreement with the small torsional angle (55.5°, mean). The bridgehead OCH signal [δ(H) 4.35] is a broad triplet, resulting from the coupling with $NCH_{eq}H_{ax}$ and "w" coupling to its sibling proton. The ^{1}H signals of the cbdca ligand are the typical triplet (δ 2.87) and quintet (δ 1.90); however, these become overlaid over time by other multiplets, which appear to follow from the slow H/D exchange of the cyclobutane ring with the solvent. The assignments have been confirmed by C,H-correlated NMR.

The ^{1}H and ^{13}C NMR spectra of a solution of **C1** in DMSO-d_6 (Figures S6 and S7) revealed the presence of two components in a 1:2 ratio (eq 5). The minor component is considered to be the neutral and C_{2v}-symmetrical **C1**. While its NH signal is at δ(H) 6.90, all other **C** signals of **C1**, including the ^{13}C signals, concur with those of **C2**. The signals of the major component are attributed to the ionic [{$OC_6H_{10}(NH)_2$}-$PtCl(S(O)Me_2)$]Cl (**C1-DMSO**), which displays inequivalent amino groups and is thus of lower symmetry (C_s). For the ionic **C1-DMSO**, the two NH signals at δ(H) 7.39 and 6.30 flank that of **C1** with very similar intensity. There are two sets of signals for $NCH_{eq}H_{ax}$ and $N'CH_{eq}H_{ax}$ well separated from another and for which H_{ax} occurs at higher field than H_{eq}. In the ^{13}C NMR spectrum of **C1-DMSO**, three signals of equal intensity are found for CH, NC, and N′C. The assignments of the ^{1}H signals of **C1** and **C1-DMSO** were verified by H,H- and C,H-correlated NMR (Figures S8 and S9).

Crystal and Molecular Structure of {$OC_6H_{10}(NH)_2$}$PtCl_2$ (C1). A summary of the crystal structure determination of **C1** is included in Table 1, and representations of the structure are shown in Figure 3. The compound crystallizes in the

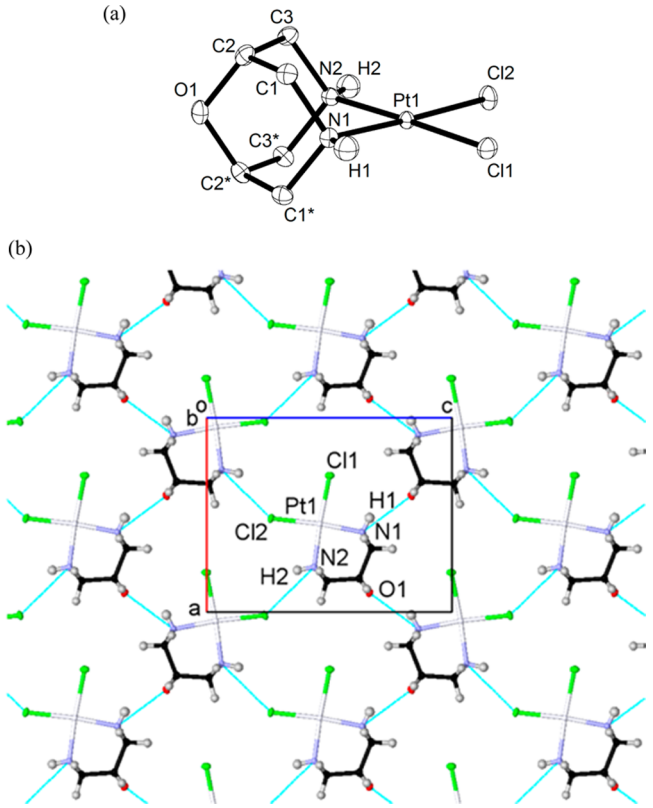

Figure 3. Crystal and molecular structure of **C1**: (a) drawing of the structure of the molecule; (b) view along the *b* axis, showing the 2D network of molecules in a plane parallel to *ac*. Selected bond distances (Å), nonbonding distances (Å), and bond angles (deg): Pt1−N1 = 2.029(2), Pt1−N2 = 2.032(2), Pt1−Cl1 = 2.3115(9), Pt1−Cl2 = 2.3107(7), C2−O1 = 1.440(2), C1−N1 = 1.490(2), C3−N2 = 1.490(2), N1···N2 = 2.779(2), C2···C2* = 2.357(2), C1···C1* = 2.433(2), C3···C3* = 2.421(2), C1···C3 = 2.579(2); C2−O1−C2* = 109.8(2), N1−Pt1−N2 = 86.36(7), Cl1−Pt1−Cl2 = 94.92(2).

orthorhombic crystal system, space group *Pnma* (No. 62), with four identical molecules in the unit cell. The space group of solid **C1** is different from that of the homologues {$C_7H_{12}(NH)_2$}$PtCl_2$ (**A1**)[14] and {$F_2C_7H_{10}(NH)_2$}$PtCl_2$ (**D1**) [both $P2_1/n$ (No. 14)][16] and {$(HO)_2C_7H_{10}(NH)_2$}$PtCl_2$ [**B1**; $C2/c$ (No. 15)].[15]

The Pt−N bond lengths in **C1** are 2.029(2) and 2.032(2) Å and thus lie within the typical range for (bispidene)platinum-(II) complexes (2.02−2.04 Å); the same holds for the Pt−Cl bonds at 2.311(2) Å (mean). Upon coordination of **C** to $PtCl_2$, the N···N distance reduces from 2.875(3) Å (**C**) to 2.779(2) Å

DOI: 10.1021/acs.inorgchem.6b01690
Inorg. Chem. XXXX, XXX, XXX−XXX

in **C1**, which marks the upper limit of the range of distances (2.76−2.78 Å)[14] for complexes of this kind. Accordingly, the N−Pt−N angle opens to 86.4(1)° (from 85.3 to 85.8° in **A1**, **B2**, and **D2**). Coordination of **C** at $PtCl_2$ goes along with slight widening of the C2···C5 distance from 2.344(3) Å in **C** to 2.357(2) Å in **C1** (here C2···C2*), but this distance, nevertheless, remains markedly shorter than that for (9-*C*-bispidine)platinum(II) complexes (2.46−2.47 Å). Thus, all in all, the **C** ligand in **C1** appears quite contracted compared to the other bispidines.

In the crystal of **C1**, molecules reside on crystallographic mirror planes that pass through the atom O1, both NH groups, the Pt atom, and the two chloride ligands. Neighboring molecules in each plane are related by two 2-fold screw axes along *a* and the glide planes parallel to *ab*. The molecules are hydrogen-bonded to their neighbors to one side by N−H···Cl hydrogen bonds {N2−H2···Cl2 = 2.60(4) Å [137(2)°; N2···Cl2 = 3.239(2) Å]} and to the other side by N−H···O hydrogen bonds {N1−H1···O1 = 2.21(4) Å [145(2)°; N1···O1 = 2.847(2) Å]}. In this way, strictly planar 2D networks are formed (Figure 3b).

Contiguous planes are stacked along *b* at a distance of *b*/2 = 4.5424 Å to one another. The molecules are related to their closest neighbors in the adjacent planes by 2 × 2 screw axes along *b*. There appears to be only a weak vdW interaction between the molecules in different planes, probably supported by additional N2C3−H3B···Cl1 = 2.67(4) Å [148(2)°; C3···Cl1 = 3.550(2) Å] hydrogen-bonding interactions involving the chloride Cl1, which is not taking part in the planar networks.

According to the structural data, the molecular volume of **C1** is $V/Z = V_m$ = 236.7 Å^3, which is distinctly less than that of parent **A1** at V_m = 252.2 Å (ΔV_m = −15.5 Å^3).[14] The reduction of the volume reflects roughly the difference in the molecular volumes of the uncoordinated bispidines **A** (V_m = 180.2 Å^3)[13] and **C** (V_m = 165.5 Å^3; ΔV_m = −14.7 Å^3).

Crystal and Molecular Structure of $\{OC_6H_{10}(NH)_2\}$Pt-$\{C_4H_6(CO_2)_2\}\cdot 5H_2O$ (C2). The crystal structure of the (9-oxabispidine)platinum complex **C2** [Table 1; triclinic crystal system, space group $P\bar{1}$ (No. 2)] is isomorphous to those of the parent bispidine $\{C_7H_{12}(NH)_2\}Pt\{C_4H_6(CO_2)_2\}\cdot 5H_2O$ (**A2**; compound **2b** in ref 14), and 9,9-difluorobispidine $\{F_2C_7H_{10}(NH)_2\}Pt\{C_4H_6(CO_2)_2\}\cdot 5H_2O$ (**D2**),[16], whereas the corresponding 9,9-diol $\{(HO)_2C_7H_{10}(NH)_2\}Pt\{C_4H_6(CO_2)_2\}\cdot 2H_2O$ [**B2**; tetragonal, $P4/n$ (No. 85)] differs in the hydrate content. There are two independent platinum complexes and 10 water molecules in the asymmetric unit of **C2**, so the unit cell (Z = 2) contains a total of four platinum complexes and 20 water molecules (Figure 4). The packing of the molecules in the crystal is essentially based on hydrogen bonding between the complex molecules and water and is determined by the eight inversion centers of the space group. Each platinum complex is completely surrounded by a shell of water molecules, and there are no direct bonds between neighboring platinum complexes. The easy hydration of the Pt(cbdca) complexes may be due to their strongly curved structure, which impedes crystallization without the incorporation of solute molecules. The structure and packing have been described in detail for **A2**.[14]

While the structure of **C2** is very similar to that of **A2** and **D2**, in particular with respect to hydrogen bonding, some features are noteworthy. (i) The ethereal O atom of the **C** ligand in **C2** is not involved in any hydrogen bonding, thus illustrating the structural similarity with the other 9-substituted

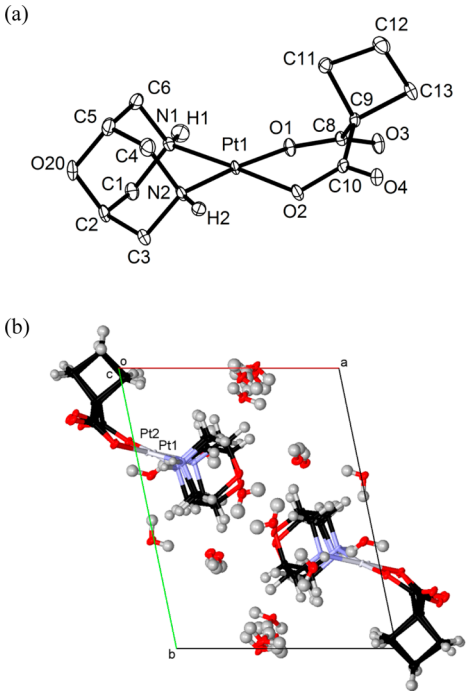

Figure 4. Crystal and molecular structure of **C2**: (a) drawing of the structure of molecule 1; (b) packing of the molecules in the crystal. Selected bond distances (Å), nonbonding distances (Å), and bond angles (deg); molecule 1, Pt1−N1 = 2.025(2), Pt1−N2 = 2.026(2), Pt1−O1 = 2.036(2), Pt1−O2 = 2.017(2), N1···N2 = 2.788(3), C2···C5 2.351(4), N1−Pt1−N2 = 87.0(1), O1−Pt1−O2 = 90.4(1); molecule 2, Pt2−N3 = 2.019(2), Pt2−N4 = 2.024(3), Pt2−O5 = 2.027(2), Pt2−O6 = 2.025(2), N3···N4 = 2.790(3), C15···C18 2.360(4), N3−Pt2−N4 = 87.3(1), O5−Pt2−O6 = 89.3(1).

derivatives. (ii) The C−O20/21 bonds of **C2** [1.444(2) Å, mean] are shorter than the respective C−C bonds in **A2** [1.532(2) Å, mean] and **D2** [1.517(5) Å, mean], involving the bridging atom of the bispidine ligands. This leads to compression of the ligand, as is evident from the shorter intramolecular distances between the bridgehead atoms C2···C5 = 2.351(4) Å and C15···C18 = 2.360(4) Å, as has also been found for the dichloride **C1** [2.357(2) Å]. (iii) As is evident from the larger nonbonding N···N distances at 2.789(3) Å (mean) and the larger N−Pt−N angles at 87.1(2)°, the "bite" of the **C** ligand in **C2** is still further increased compared to those of **C1** [2.779(2) Å and 86.4(1)°] and the parent **A2** [2.77(1) Å and 86.4(3)°]. (iv) As a consequence of 9-O, the volume of the formula unit (V/Z) of **C2** at 463.6 Å^3 is lower than that of **A2** (471.0 Å^3),[14] but the difference (ΔV = −7.4 Å^3) is less than that expected from the Hofmann atom volume increments (ΔV_{calc} = −12.64 Å^3; see **C**), so the hydrate shell appears to cancel out part of the effect of replacement of the groups at 9-C.

3. CONCLUSIONS

Continuing our ongoing study of the (bispidine)platinum(II) analogues of cisplatin, carboplatin, and oxaliplatin, we have revisited the literature synthesis of **C** and prepared and investigated a series of new platinum(II) complexes containing **C** as the carrier ligand. Essential findings from this study are as follows:

(i) The literature synthesis of **C** has been improved. Pure **C** can now be prepared efficiently on a gram scale. **C** has been

DOI: 10.1021/acs.inorgchem.6b01690
Inorg. Chem. XXXX, XXX, XXX−XXX

characterized in detail, including the determination of its X-ray crystal structure.

(ii) The 9-oxabispidine complexes **C1**−**C3** have been synthesized. Both **C1** and **C2** have been characterized by crystal structure analysis. While the dichloride **C1** is only sparingly soluble in water and the oxalate **C3** is practically insoluble, the pentahydrate **C2** dissolves well.

(iii) An important feature of **C** and its complexes is the reduced size of **C** (uncoordinated or as a ligand) compared to the usual bispidines because of the short C−O bonds. The intramolecular distance between the tertiary C atoms and the molecular volume V_m determined from structural data allow the bulk of **C** to be assessed.

(iv) The introduction of the ether group into the bridging position of bispidine causes an increase of the acidity of the NH protons, which strengthens the N−H···X (X = N, Cl, O) bridge bonds in the solid. The strengthening of these bonds appears to contribute to reduced solubility, in particular of **C1** and **C3**, in all solvents, including water.

(v) Although the ethereal 9-O atom of **C** is a base and possible hydrogen-bond acceptor for NH, it is only partially involved in the packing of the molecules in the crystals, either uncoordinated (**C**) or as a ligand (in **C2**). The most notable interaction is in the 2D network structure of **C1**.

(vi) We found that the (9-oxabispidine)platinum complexes **C1**−**C3** express markedly lower cytotoxic potency to the ovarian cancer cell line A2780 than the parental bispidine complexes **A1**−**A3**.[30] This feature is attributed to an increased polarity of the bonds in the **C** skeleton caused by the high electronegativity of O, which appears to decrease the lipophilicity of the compounds.

4. EXPERIMENTAL SECTION

The reactions were performed with Schlenk-type glassware under argon. (1,5-Hexadiene)platinum dichloride[25] was prepared according to the literature. A revised protocol for the synthesis of 9-oxabispidine (**C**, $C_6H_{12}N_2O$, fw 128.2) is included in the SI.

(9-Oxabispidine)platinum(II) Dichloride (C1). A solution of **C** (0.555 g, 4.33 mmol) in 100 mL of DMF was added to (1,5-hexadiene)platinum dichloride (1.66 g, 4.77 mmol), and the mixture was heated to 65 °C overnight. The solution adopted a light-green color, and a greenish-yellow solid precipitated: yield 1.17 g (2.97 mmol, 69%). ESI$^+$ MS (MeOH): *m/e* 416 ([M + Na]$^+$, 100%), 809 ([2M + Na]$^+$, 45%). ^{1}H NMR (DMSO-d_6, 600 MHz): δ 6.90 (s, 2H, NH), 4.09 ("s", 2H, CH), 3.27 (d, 4H, $NCH_{ax}H_{eq}$), 3.07 (m, 4H, $NCH_{ax}H_{eq}$). ^{13}C NMR (DMSO-d_6): δ 64.2 (2C, CH), 51.1 (4C, NCH_2). Anal. Calcd for $C_6H_{12}Cl_2N_2OPt$ (394.2): C, 18.28; H, 3.07; Cl, 17.99; N, 7.11; O, 4.06; Pt, 49.49. Found: C, 18.31; H, 3.04; Cl, 17.95; N, 7.07; Pt, 49.47.

[{$OC_6H_{10}(NH)_2$}PtCl(DMSO)]Cl (C1-DMSO). ^{1}H NMR (DMSO-d_6, 600 MHz): δ 7.39, 6.30 (each s, 1H, NH), 4.23 ("s", 2H, CH), 3.48 (d, 4H, $NCH_{ax}H_{eq}$), 3.37 (m, 4H, $NCH_{ax}H_{eq}$), 3.19 (d, 4H, $N'CH_{ax}H_{eq}$), 3.09 (m, 4H, $N'CH_{ax}H_{eq}$). ^{13}C NMR (DMSO-d_6): δ 64.1 (2C, CH), 51.4 (2C, NCH_2), 49.7 (2C, $N'CH_2$).

(9-Oxabispidine)platinum(II) Cyclobutane-1,1-dicarboxylate (C2). A suspension of **C1** (394 mg, 1.00 mmol) and $(AgO_2C)_2C_4H_6$ (358 mg, 1.00 mmol) in 40 mL of H_2O was stirred and protected from light for 24 h. After filtration to remove AgCl, the water was evaporated. The solid was dried under reduced pressure to yield colorless **C2**: 275 mg (59%). Recrystallization from hot water (70 °C) afforded colorless crystals of the pentahydrate, which collapse upon removal of the solvent. Crystals for X-ray structure determination have been selected directly from the aqueous solution and sealed with perfluoropolyether Fomblin Y (Sigma-Aldrich): $C_{12}H_{18}N_2O_5Pt$ (465.4). ESI$^+$ MS (MeOH/H_2O): *m/e* 488 ([M + Na]$^+$, 100%). ^{1}H NMR (D_2O, 600 MHz): δ 4.35 ("t", 2H, CH), 3.51 (d, ^2J(HH) = 13.2 Hz, 4H, $NCH_{ax}H_{eq}$), 3.37 (dd, ^2J(HH) = 13.2 Hz, ^3J(HH) = 3.5 Hz, 4H, $NCH_{ax}H_{eq}$), oxabispidine; 2.87 (t, ^3J(HH) = 8 Hz, 4H, CH_2), 1.90 (quint, ^3J(HH) = 8 Hz, 2H, CH_2), cbdca. ^{13}C NMR (D_2O): δ 65.4 (2C, CH), 51.9 (4C, NCH_2), oxabispidine; 181.8 (2C, CO_2), 56.2 (1C, C_{quat}), 31.0 (2C, CH_2), 15.3 (1C, CH_2), cbdca. Anal. Calcd for $C_{12}H_{18}N_2O_5Pt{\cdot}H_2O$ (483.4): C, 29.82; H, 4.17; N, 5.80; O, 19.86; Pt, 40.36. Found: C, 29.38; H, 4.14; N, 5.88; Pt, 41.03.

(9-Oxabispidine)platinum(II) Oxalate (C3). $Na_2C_2O_4$ (145 mg, 1.08 mmol) was added to a light-yellow suspension of **C1** (394 mg, 1.00 mmol) in 100 mL of H_2O. The mixture was stirred at 40 °C overnight, whereupon the color faded. The nearly white solid was isolated by filtration, washed with water, and dried under vacuum: yield 275 mg (67%). Recrystallization from hot water (70 °C) afforded off-white microcrystals of **C3**, however with a marked loss of material. ESI$^+$ MS (MeOH): *m/e* 434 ([M + Na]$^+$, 100%) (high background noise due to low solubility). Anal. Calcd for $C_8H_{12}N_2O_5Pt$ (411.3): C, 23.36; H, 2.94; N, 6.81; Pt, 47.43. Found: C, 23.40; H, 2.96; N, 6.78; Pt, 47.41. No NMR spectra were recorded owing to insolubility.

■ ASSOCIATED CONTENT

Supporting Information

The Supporting Information is available free of charge on the ACS Publications website at DOI: 10.1021/acs.inorgchem.6b01690.

Protocols for the synthesis of **I**−**VI**, including the NMR characterization of **cis-III** and **trans-III** and the X-ray structure analysis of **trans-III**, IR spectra of all new compounds, and NMR spectra of **C1** and **C2** (PDF)

X-ray crystallographic data in CIF format for **V**$^{\bullet}$$^{1}/_{2}$**py** (CCDC 1491344), **C** (CCDC 1491345), **C1** (CCDC 1491346), **C2** (CCDC 1491347), and **trans-III** (CCDC 1491348) (CIF)

■ AUTHOR INFORMATION

Corresponding Author

*E-mail: poerschke@kofo.mpg.de.

Author Contributions

All authors contributed to the writing of this manuscript.

Notes

The authors declare no competing financial interest.

■ ACKNOWLEDGMENTS

We thank Angelika Dreier and Alexander Zwerschke for technical assistance, Dr. Christophe Farès for NMR support, and Dr. Alexandra Hamacher and Professor Mathias U. Kassack from the University of Düsseldorf for the cell studies. General funding by the Max Planck Society is gratefully acknowledged.

■ REFERENCES

(1) (a) Rosenberg, B.; Van Camp, L.; Krigas, T. Inhibition of Cell Division in *Escherichia coli* by Electrolysis Products from a Platinum Electrode. *Nature* **1965**, *205*, 698−699. (b) Rosenberg, B.; Van Camp, L.; Trosko, J. E.; Mansour, V. H. Platinum Compounds: a New Class of Potent Antitumour Agents. *Nature* **1969**, *222*, 385−386. (c) Rosenberg, B.; Van Camp, L. The Successful Regression of Large Solid Sarcoma 180 Tumors by Platinum Compounds. *Cancer Res.* **1970**, *30*, 1799−1802. (d) Rosenberg, B. Some Biological Effects of Platinum Compounds. *Platinum Met. Rev.* **1971**, *15*, 42−51. (e) Rosenberg, B. Platinum Complexes for Treatment of Cancer. *Interdiscip. Sci. Rev.* **1978**, *3*, 134−147. (f) Rosenberg, B. In *Nucleic Acid−Metal Ion Interactions*; Spiro, T. G., Ed.; Wiley: New York, 1980; pp 1−29. (g) Hoeschele, J. D. In Remembrance of Barnett Rosenberg. *Dalton Trans.* **2009**, 10648−10650. (h) Muggia, F. M.; Bonetti, A.; Hoeschele, J. D.; Rozencweig, M.; Howell, S. B. Platinum Antitumor

DOI: 10.1021/acs.inorgchem.6b01690
Inorg. Chem. XXXX, XXX, XXX−XXX

Complexes: 50 Years Since Barnett Rosenberg's Discovery. *J. Clin. Oncol.* **2015**, *33*, 4219−4226.
(2) (a) Harrison, R. C.; McAuliffe, C. A.; Zaki, A. M. An Efficient Route for the Preparation of Highly Soluble Platinum(II) Antitumour Agents. *Inorg. Chim. Acta* **1980**, *46*, L15−L16. (b) Neidle, S.; Ismail, I. M.; Sadler, P. J. The Structure of the Antitumor Complex Cis-(diammino)(1,1-cyclobutanedicarboxylato)Pt(II): X-Ray and NMR Studies. *J. Inorg. Biochem.* **1980**, *13*, 205−212. (c) Beagley, B.; Cruickshank, D. W. J.; McAuliffe, C. A.; Pritchard, R. G.; Zaki, A. M.; Beddoes, R. L.; Cernik, R. J.; Mills, O. S. The Crystal and Molecular Structure of Cis-diammine-1,1-cyclobutanedicarboxoplatinum(II) [cis-$Pt(NH_3)_2$CBDCA]. Dynamic Puckering of the Cyclobutane Ring. *J. Mol. Struct.* **1985**, *130*, 97−102.
(3) Galanski, M.; Jakupec, M. A.; Keppler, B. K. Oxaliplatin and Derivatives as Anticancer Drugs−Novel Design Strategies. In *Metal Compounds in Cancer Chemotherapy*; Pérez, J. M., Fuertes, M. A., Alonso, C., Eds.; Research Signpost: Trivandrum, India, 2005; pp 155−186.
(4) (a) Cleare, M. J.; Hoeschele, J. D. Studies on the Antitumor Activity of Group VIII Transition Metal Complexes. Part I. Platinum(II) Complexes. *Bioinorg. Chem.* **1973**, *2*, 187−210. (b) Cleare, M. J.; Hoeschele, J. D. Anti-tumour Platinum Compounds. Relationship Between Structure and Activity. *Platinum Met. Rev.* **1973**, *17*, 2−13. (c) Cleare, M. J. Transition Metal Complexes in Cancer Chemotherapy. *Coord. Chem. Rev.* **1974**, *12*, 349−405. (d) Cleare, M. J.; Hydes, P. C.; Malerbi, B. W.; Watkins, D. M. Anti-tumour Platinum Complexes: Relationships Between Chemical Properties and Activity. *Biochimie* **1978**, *60*, 835−850. (e) Connors, T. A.; Cleare, M. J.; Harrap, K. R. Structure-Activity Relationships of the Antitumor Platinum Coordination Complexes. *Cancer Treat. Rep.* **1979**, *63*, 1499−1502. (f) van der Veer, J. L.; Reedijk, J. Investigating Antitumour Drug Mechanisms. *Chem. Br.* **1988**, *24*, 775−780. (g) de Mier-Vinué, J.; Montaña, A. M.; Moreno, V. Platinum Complexes with Cytotoxic Activity: Models for Structure−Activity Relationship Studies. In *Metal Compounds in Cancer Chemotherapy*; Pérez, J. M., Fuertes, M. A., Alonso, C., Eds.; Research Signpost: Trivandrum, India, 2005; pp 47−154. (h) Montaña, A. M.; Batalla, C. The Rational Design of Anticancer Platinum Complexes: The Importance of the Structure-Activity Relationship. *Curr. Med. Chem.* **2009**, *16*, 2235−2260.
(5) (a) Kelland, L. The Resurgence of Platinum-based Cancer Chemotherapy. *Nat. Rev. Cancer* **2007**, *7*, 573−584. (b) Wilson, J. J.; Lippard, S. J. Synthetic Methods for the Preparation of Platinum Anticancer Complexes. *Chem. Rev.* **2014**, *114*, 4470−4495. (c) Farrell, N. P. Multi-platinum Anti-cancer Agents. Substitution-inert Compounds for Tumor Selectivity and New Targets. *Chem. Soc. Rev.* **2015**, *44*, 8773−8785.
(6) (a) Fanelli, M.; Formica, M.; Fusi, V.; Giorgi, L.; Micheloni, M.; Paoli, P. New Trends in Platinum and Palladium Complexes as Antineoplastic Agents. *Coord. Chem. Rev.* **2016**, *310*, 41−79. (b) Johnstone, T. C.; Suntharalingam, K.; Lippard, S. J. The Next Generation of Platinum Drugs: Targeted Pt(II) Agents, Nanoparticle Delivery, and Pt(IV) Prodrugs. *Chem. Rev.* **2016**, *116*, 3436−3486. (c) Gibson, D. Platinum(IV) Anticancer Prodrugs − Hypotheses and Facts. *Dalton Trans.* **2016**, *45*, 12983−12991.
(7) The generally poorly water-soluble cisplatin-type drugs can be assumed to be partially self-associated when passing through the cell membrane and entering the cell fluid due to hydrogen bonding of the NH groups to anionic sites. These oligomeric entities must be cleaved by hydrogen bonding to water and other bases in the cell fluid, apart from ion dissociation of the compounds. By undergoing a multitude of such equilibria with involvement of the NH functions, the drug is thought to move on to select the DNA sites for the final destination. Some of these aspects have been addressed, but a more detailed picture still seems desirable. (a) Reedijk, J. Why Does Cisplatin Reach Guanine-N7 With Competing S-Donor Ligands Available in the Cell? *Chem. Rev.* **1999**, *99*, 2499−2510. (b) Reedijk, J. Metal-Ligand Exchange Kinetics in Platinum and Ruthenium Complexes. *Platinum Met. Rev.* **2008**, *52*, 2−11. (c) Miguel, P. J. S.; Roitzsch, M.; Yin, L.; Lax, P. M.; Holland, L.; Krizanovic, O.; Lutterbeck, M.; Schürmann, M.; Fusch, E. C.; Lippert, B. On the Many Roles of NH_3 Ligands in Mono- and Multinuclear Complexes of Platinum. *Dalton Trans.* **2009**, 10774−10786.
(8) Haack, K.-J.; Goddard, R.; Pörschke, K.-R. Applying the Macrocyclic Effect to Smaller Ring Structures. *N,N′*-Dimethyl-3,7-diazabicyclo[3.3.1]nonane Nickel(0) Complexes. *J. Am. Chem. Soc.* **1997**, *119*, 7992−7999.
(9) (a) Izatt, R. M.; Bradshaw, J. S.; Nielsen, S. A.; Lamb, J. D.; Christensen, J.; Sen, D. Thermodynamic and Kinetic Data for Cation−Macrocycle Interaction. *Chem. Rev.* **1985**, *85*, 271−339. (b) Hancock, R. D.; Martell, A. E. The Chelate, Cryptate and Macrocyclic Effects. *Comments Inorg. Chem.* **1988**, *6*, 237−284 and references cited therein..
(10) Tomassoli, I.; Gündisch, D. Bispidine as a Privileged Scaffold. *Curr. Top. Med. Chem.* **2016**, *16*, 1314−1342.
(11) Miyahara, Y.; Goto, K.; Inazu, T. Convenient Synthesis of 3,7-Diazabicyclo[3.3.1]nonane (Bispidine). *Synthesis* **2001**, *2001*, 364−366.
(12) Cui, H.; Goddard, R.; Pörschke, K.-R. Synthesis and Coordination Chemistry of *N,N*-Diallylbispidine. *Organometallics* **2011**, *30*, 6241−6252.
(13) Cui, H.; Goddard, R.; Pörschke, K.-R. Degradation of Dichloromethane by Bispidine. *J. Phys. Org. Chem.* **2012**, *25*, 814−827.
(14) Cui, H.; Goddard, R.; Pörschke, K.-R.; Hamacher, A.; Kassack, M. U. Bispidine Analogues of Cisplatin, Carboplatin, and Oxaliplatin. Synthesis, Structures, and Cytotoxicity. *Inorg. Chem.* **2014**, *53*, 3371−3384.
(15) Cui, H.; Goddard, R.; Pörschke, K.-R.; Hamacher, A.; Kassack, M. U. Bispidin-9,9-diol Analogues of Cisplatin, Carboplatin, and Oxaliplatin: Synthesis, Structures, and Cytotoxicity. *Inorg. Chem.* **2016**, *55*, 2986−2997.
(16) Mitra, R.; Goddard, R.; Pörschke, K.-R. 9,9-Difluorbispidine Analogs of Cisplatin, Carboplatin, and Oxaliplatin. In preparation.
(17) Stetter, H.; Meissner, H.-J. Synthese des 1.3-Diaza-6-oxa-adamantans. *Chem. Ber.* **1963**, *96*, 2827−2830.
(18) Budzikiewicz, H.; Djerassi, C.; Williams, D. H. *Mass Spectrometry of Organic Compounds*; Holden-Day: San Francisco, CA, 1967; pp 297−335.
(19) In six-membered hydrocarbon rings, the axial protons usually resonate at higher field than the equatorial protons. It has been noted before that this sequence can be reversed when heteroatoms (in particular S) are part of the ring. (a) Klepikova, S. G.; Yu, V. K.; Fomicheva, E. E.; Mukhasheva, R. D.; Praliev, K. D.; Berlin, K. D. ^{1}H NMR Spectroscopy in the Study of the Three-dimensional Structure of 7-Alkoxyalkyl-3-thia-7-azabicyclo[3.3.1]nonan-9-ones and Some of Their Derivatives. *Chem. Heterocycl. Compd.* **2008**, *44*, 1398−1403. (b) Yu, V. K.; Berlin, K. D.; Iskakova, T. K.; Faskhutdinov, M. F.; Praliyev, K. D.; Lee, C. P.; Ten, A. Y.; Malmkova, A. Y. Unusual Conformational Behavior of 3,7-Dihetera(N,N-;N,O-;N,S-)-bicyclo[3.3.1]nonan-9-ols Via NMR Analysis. *Phosphorus, Sulfur Silicon Relat. Elem.* **2014**, *189*, 864−872.
(20) Brun, S.; Torres, Ò.; Pla-Quintana, A.; Roglans, A.; Goddard, R.; Pörschke, K.-R. Nickel(0) Complexes of Acyclic Polyunsaturated Aza Ligands. *Organometallics* **2013**, *32*, 1710−1720.
(21) Bispidine (**A**) crystallizes from pentane (−40 °C) in the orthorhombic crystal system, space group $P2_12_12_1$ (No. 19).[13] All molecules are nonsymmetric and of the same enantiomeric conformation. The four molecules in the unit cell are pairwise head−tail associated by N2−H2···N1* hydrogen bonds, forming zigzag chains along two 2-fold screw axes parallel to the *c* axis that run in opposite directions.
(22) Etter, M. C. Encoding and Decoding Hydrogen-bond Patterns of Organic Compounds. *Acc. Chem. Res.* **1990**, *23*, 120−126.
(23) (a) Bondi, A. Van der Waals Volumes and Radii. *J. Phys. Chem.* **1964**, *68*, 441−451. (b) Mantina, M.; Chamberlin, A. C.; Valero, R.; Cramer, C. J.; Truhlar, D. G. Consistent van der Waals Radii for the Whole Main Group. *J. Phys. Chem. A* **2009**, *113*, 5806−5812.
(24) Hofmann, D. W. M. Fast Estimation of Crystal Densities. *Acta Crystallogr., Sect. B: Struct. Sci.* **2002**, *57*, 489−493.

DOI: 10.1021/acs.inorgchem.6b01690
Inorg. Chem. XXXX, XXX, XXX−XXX

(25) (a) Jensen, K. A.; Nielsen, E. J.; Reiter, R.; Schonfeldt, E.; Steensgaard, I.; Rosenberg, Th. Platinum Compounds of Alkadienes (Diolefins). *Acta Chem. Scand.* **1953**, *7*, 866−868. (b) Garcia, L.; Shupack, S. I.; Orchin, M. Preparation and Reactions of Olefin−Pyridine N-Oxide Platinum(II) Complexes. *Inorg. Chem.* **1962**, *1*, 893−896. (c) Deacon, G. B.; Nelson-Reed, K. T. Preparations and Ligand Displacement-Reactions of Diene(polyfluorophenyl)platinum-(II) Complexes. *J. Organomet. Chem.* **1987**, *322*, 257−268. (d) Nair, R. N.; Golen, J. A.; Rheingold, A. L.; Grotjahn, D. B. Unexpected Synthesis and Structural Characterization of Pt(II)Cl_2-1,5-hexadiene from Reaction of Allyl chloride and K_2PtCl_4. *Inorg. Chim. Acta* **2010**, *364*, 272−274.

(26) (a) Kerrison, S. J. S.; Sadler, P. J. Solvolysis of *cis*-$[Pt(NH_3)_2Cl_2]$ in Dimethyl Sulphoxide and Reactions of Glycine with $[PtCl_3(Me_2SO)]^-$ as Probed by ^{195}Pt Nuclear Magnetic Resonance Shifts and ^{195}Pt−^{15}N Coupling Constants. *J. Chem. Soc., Chem. Commun.* **1977**, 861−863. (b) Fanizzi, F. P.; Intini, F. P.; Maresca, L.; Natile, G.; Uccello-Barretta, G. Solvolysis of Platinum Complexes with Substituted Ethylenediamines in Dimethyl Sulfoxide. *Inorg. Chem.* **1990**, *29*, 29−33. (c) Farrell, N.; Kiley, D. M.; Schmidt, W.; Hacker, M. P. Chemical Properties and Antitumor Activity of Complexes of Platinum Containing Substituted Sulfoxides [PtCl(R′R″SO)(diamine)]NO_3. Chirality and Leaving-Group Ability of Sulfoxide Affecting Biological Activity. *Inorg. Chem.* **1990**, *29*, 397−403.

(27) For the impact of DMSO on the cytotoxicity of cisplatin-type drugs, see: (a) Fischer, S. J.; Benson, L. M.; Fauq, A.; Naylor, S.; Windebank, A. J. Cisplatin and Dimethyl Sulfoxide React to Form an Adducted Compound with Reduced Cytotoxicity and Neurotoxicity. *NeuroToxicology* **2008**, *29*, 444−452. (b) Hall, M. D.; Telma, K. A.; Chang, K.-E.; Lee, T. D.; Madigan, J. P.; Lloyd, J. R.; Goldlust, I. S.; Hoeschele, J. D.; Gottesman, M. M. Say No to DMSO: Dimethylsulfoxide Inactivates Cisplatin, Carboplatin, and Other Platinum Complexes. *Cancer Res.* **2014**, *74*, 3913−3922.

(28) Silverstein, R. M.; Webster, F. X.; Kiemle, D. J. *Spectrometric Identification of Organic Compounds*, 7th ed.; Wiley: Hoboken, NJ, 2005; pp 72−133.

(29) (a) Bohlmann, F. Zur Konfigurationsbestimmung von Chinolizin-Derivaten. *Angew. Chem.* **1957**, *69*, 641−642. (b) Bohlmann, F. Lupinen-Alkaloide. 8. Zur Konfigurationsbestimmung von Chinolizidin-Derivaten. *Chem. Ber.* **1958**, *91*, 2157−2167. (c) Hamlow, H. P.; Okuda, S.; Nakagawa, N. NMR Effects of Cyclic Tertiary Amines. *Tetrahedron Lett.* **1964**, *5*, 2553−2559. (d) Bohlmann, F.; Schumann, D.; Schulz, H. Über die NMR-Spektren von Chinolizidin-Derivaten. *Tetrahedron Lett.* **1965**, *6*, 173−177. (e) Skolik, J.; Krüger, P. J.; Wiewiorowski, M. Correlation Between the Stereochemistry of Quinolizidine Alkaloids and Their Infrared Spectra from 2840−2600 cm^{-1}. *Tetrahedron* **1968**, *24*, 5439−5456. (f) Lambert, J. B.; Keske, R. G.; Carhart, R. E.; Jovanovich, A. P. The Conformational Rivalry between the Nonbonding Electron Pair and the Proton on Nitrogen. *J. Am. Chem. Soc.* **1967**, *89*, 3761−3767. (g) Crabb, T. A.; Jones, E. R. Proton Magnetic Resonance Studies of Compounds with Bridgehead Nitrogen Atoms−XII. *Tetrahedron* **1970**, *26*, 1217−1233. (h) Jeyaraman, R.; Ravindran, T.; Sujatha, M.; Venkatraj, M. Lowering of Bohlmann Band Intensities in Conformationally Homogeneous 2,6-Diarylpiperidines Due to Ring Distortion. *Ind. J. Chem., Sect. B* **1999**, *38*, 52−55.

(30) Cytotoxicity of the new compounds was determined with MTT assay against the human ovarian cancer cell line A2780 and its cisplatin-resistant subline A2780 CisR. The compounds showed no significant cytotoxic effects at concentrations lower than 100 μM. For details of the testing procedure, see ref 14.

DOI: 10.1021/acs.inorgchem.6b01690
Inorg. Chem. XXXX, XXX, XXX−XXX